CSIRO PUBLISHING

The Rangeland Journal, 2021, **43**, 285–295
https://doi.org/10.1071/RJ20073

A new net primary productivity model and new management strategy of grassland classification based on CSCS in China

Huilong Lin[A,B], *Haili Ma*[A], *Charles Nyandwi*[A], *Qisheng Feng*[A] and *Tiangang Liang*[A]

[A]State Key Laboratory of Grassland Agro-ecosystems, Key Laboratory of Grassland Livestock Industry Innovation, Ministry of Agriculture and Rural Affairs; College of Pastoral Agriculture Science and Technology, Lanzhou University, Lanzhou 730020, China.
[B]Corresponding author. Email: linhuilong@lzu.edu.cn

Abstract. The discovery of grassland field, form and biomass in China was central to the sustainable development of grassland. In this study, the realistic spatial distribution patterns of grasslands were clarified through the combination of the International Geosphere-Biosphere Program (IGBP) and the Comprehensive and Sequential Classification System (CSCS). An optimal net primary productivity (NPP) model suitable for Chinese grasslands was introduced by integrating the classification indices-based model (CIM) with the Normalised Difference Vegetation Index (NDVI), and comparing it with the standard classical model (Miami, Schuur, CIM, CASA model). Using the optimal model as the algorithm basis, the net primary production spatial pattern of grassland in China was determined. The results showed that: (1) the total area of grassland was ~374.3 × 104 km^2 in 2018, mainly distributed in north-western China. Among the grassland super-class groups, Tundra and alpine steppe were largest, and Warm desert smallest; (2) the optimal modified CIM had the highest prediction efficiency, and the overall accuracy was higher than the standard classical model (Miami, Schuur, CIM, CASA model). It achieved the accurate calculation of grassland NPP in China; (3) different grassland super-class groups had different carbon fixation efficiency per unit area, resulting in huge differences in total NPP. Among the various grassland super-class groups, the temperate humid grassland, steppe, tundra and alpine steppe had high conversion efficiency per unit area of NPP, whereas that for warm desert and the savanna was low. The total NPP was 388.04×10^{12} g C/year in the study area in 2018. The results provide a basis for the rational arrangement of grassland ecological and productive functions, and are significant for developing a new strategy of grassland classification management in China.

Keywords: biomass spatial pattern, China, realistic spatial distribution patterns of grasslands, grassland ecological function, grassland productive function, NPP, simulation, rational management.

Received 19 July 2020, accepted 3 November 2020, published online 16 April 2021

Introduction

China's grassland region represents 41.7% of the total land area and is one of the most important forms of land habitat. It has substantial ecological service and productive functions, which play major roles in sustaining the terrestrial ecosystem's biodiversity and carbon cycle (Ma *et al.* 2016; Han *et al.* 2018).

The rational arrangement of the productive and ecological functions of grassland is a fundamental problem of grassland sustainable development (Shen *et al.* 2016; Liu *et al.* 2019). The basic consideration is how to achieve a balance between grassland and livestock in a country with a large grassland area of various types. The premise of achieving such a balance is to determine the grassland area, type, and biomass. Conventional methods for determining grassland areas include census, survey, and remote sensing inversion methods. However, census and survey data are often limited by the scope and time required for the survey. The remote sensing inversion method lacks detailed ground verification and has considerable uncertainty (Shen *et al.* 2016). For example, the Chinese grassland area calculated by using census and survey data methods is 280 × 104 km^2 (estimated according to the 1:1 million Chinese vegetation map (Hou 2001)), 406 × 104 km^2 (using the 1:4 million vegetation maps) (Sun 1981) and 3.5–4.3 × 106 km^2 (estimated based on clearing data (Wang *et al.* 2001; Ni 2002)). The area of grassland in China estimated by remote sensing varies substantially between studies again due to the use of different data sources and classification methods. For example, Li *et al.* (2004) estimated that the grassland area calculated using scanning radiometer data with a spatial resolution of 8 km was 166.96 km^2. Fang *et al.* (2018) estimated the grassland area from the GIMMS NDVI (Global Inventory

Modelling and Mapping Studies, normalised difference vegetation index) dataset to be ~293.05 × 104 km^2. The IGBP-LUCC (International Geosphere-Biosphere Program, IGBP; Land Use/Land Cover, LUCC) remote sensing product of the IGBP (Rosswall 1992; Friedl *et al.* 2002) could reflect vegetation types such as forest, shrub, grass, and 17 types of land cover types such as urban and built-up lands, water bodies, and permanent ice and snow. Its land-use methods have been widely recognised and applied all over the world (de Beurs and Henebry 2005; Wake 2014). However, the IGBP classification method on the grassland type system was too coarse (Liang *et al.* 2012*a*). Ren *et al.* (2008) proposed that the combination of heat and water conditions was the essential factor in grassland phenomena and processes. Based on this, the Comprehensive and Sequential Classification System (CSCS) was proposed in 1957. After continuous modification and improvement, a complete grassland classification system was developed, and its outstanding features demonstrated the genetic relationship between the categories (Ren *et al.* 2008), which provided the possibility of studying the spatial distribution of zonal grassland classes and the response to global climate change (Ren *et al.* 2008; Liang *et al.* 2012*a*, 2012*b*). In recent years, based on the CSCS, the potential distribution of grasslands have been studied on the Tibetan Plateau (Liang *et al.* 2012*b*), the entire country (Lin *et al.* 2013*a*), and the global grassland (Lin *et al.* 2012; Liang *et al.* 2012*a*, 2012*b*; Feng *et al.* 2013), reflecting the relationship between climate and vegetation changes. Xiu *et al.* (2014) used the land cover classification data (MCD12Q1) with a spatial resolution of 500 m combined with the CSCS method and found a minimum area of potential Chinese grassland of 137 × 104 km^2. However, using the CSCS method to study the spatial distribution pattern of grassland on a national scale remains uncommon. Therefore, the combination of CSCS and IGBP-LUCC provides the possibility of exploring the area and type of grasslands.

Grassland's net primary productivity (NPP) is the remainder of gross primary productivity after vegetation autotrophic respiration deduction, is the major component of biomass, and is an important ecological and production index (Wang *et al.* 2019; Xiao *et al.* 2019). Various models have been established both in China and elsewhere to study large-scale NPP, including statistical models (climate-related models), light energy utilisation models (parameter models), and physiological and ecological process models (ecosystem process models). Statistical models have been employed to estimate the NPP by establishing correlations between climatic factors such as temperature, precipitation, evapotranspiration and plant dry matter, including the Miami (Lieth 1972) and Schuur (Schuur 2003) models. Both have been widely used in developing countries because of the data availability characteristics, and both have achieved reasonable results (Schuur 2003). However, this type of model is based on the climatic factor as a theoretical basis and depends on meteorological stations; where meteorological observations are lacking, model application results in large errors. The light energy utilisation model uses light energy as the basic energy source of terrestrial life, and uses the photo-synthetically active radiation (APAR) absorbed by plants and related regulatory factors to estimate vegetation NPP (Monteith 1972). The representative model includes the CASA (Carnegie-Ames-Stanford Approach) model (Hadian *et al.* 2019; Saki *et al.* 2019). Such models consider the characteristics of both the environment and the vegetation, but details such as the value of the maximum solar energy utilisation rate, and the reliance on meteorological data are contentious (Jay *et al.* 2016; Liu *et al.* 2019). The ecosystem process model is a recent development in NPP estimation (Matsushita *et al.* 2004; Tripathi *et al.* 2018) but, because obtaining required parameters is difficult, the model is complicated, although it has been used for NPP on homogeneous patches at small spatial scales. It was most difficult to apply in developing countries (Zhu *et al.* 2005; Zhang *et al.* 2011). Lin *et al.* (2012) established a classification indices-based model (CIM) based on the CSCS classification index, combining the classification system with NPP simulation (Lin *et al.* 2012, 2013*a*, 2013*b*). By finding the specific position of a grassland class in the CSCS method, its corresponding NPP size can be determined. Their results (Lin *et al.* 2012,2013*b*) proved that the CIM can simulate the future NPP dynamic changes at national and even global scales. Wang *et al.* (2019) based on the systematic sampling of the Three-River Headwater region, constructed a new model by modifying the CIM with the NDVI, and accurately calculated grassland NPP. Accurate calculation of grassland NPP in China is of great significance to the sustainable development of grassland ecology and production. However, there have been few studies on the spatial distribution of grassland NPP in China, especially in different grassland types. A new model is necessary, obtained by modifying the CIM with the NDVI on nationwide scale. The new model will have the potential to be superior to traditional climate models such as the Miami and Schuur models, and will also be more easily applied than light energy utilisation models like CASA.

This research aimed to (1) explain the actual spatial distribution of grassland through the combination of IGBP and CSCS; (2) construct new NPP models by modifying the CIM with the NDVI by comparison with the standard classical model (Miami, Schuur, CIM, CASA model) to evaluate the optimal model appropriate for Chinese conditions; (3) determine the NPP spatial pattern of grassland in China based on the optimal model as the algorithm basis, to provide the foundation for sustainable utilisation of grassland resources and classified management strategy of Chinese grasslands.

Materials and methods

Systematic sampling

A stratified random system sampling was conducted for each grassland class in the main grassland areas of China, and a total of 3360 sample points were assessed. The distance between any two sample points was greater than 5 km (Fig. 1). Sampling was concentrated in the growing season (July–August). A global positioning system (GPS) was used to locate sample points. Three 0.5 × 0.5 m plots (replicates) were randomly arranged at each sample point, to collect all the aboveground green plants and obtain the wet weight. Plant samples were subsequently dried at 65°C for 24 h to constant weight, providing the biomass data of each sampling point. The sampling was carried out jointly by the National Animal Husbandry and Veterinary Service of the Ministry of Agriculture of the People's Republic of China and the Grass Industry System Analysis and Social Development Institute of Lanzhou University in 2004–2013 and

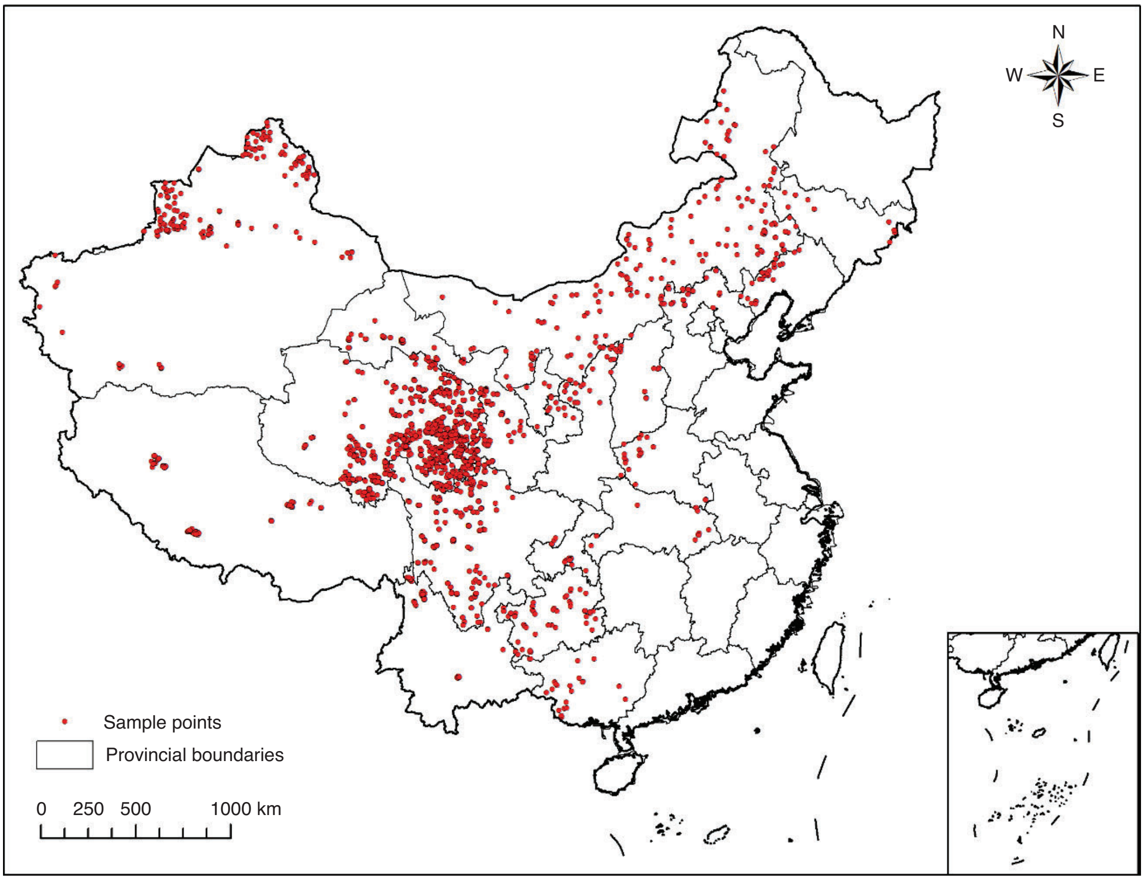

Fig. 1. Location and distribution of sampling points.

2014–2018. The measured NPP was the sum of aboveground and belowground grassland biomass (Long *et al.* 1989), where belowground biomass was estimated by the ratio coefficient (root-to-shoot ratio) of above and belowground biomass. The root: shoot ratio coefficient was derived from Piao *et al*. (2004) (see also Supplementary material Table S1, available at the journal's website). The NPP unit of measured value was g/m^2 converted to g C/m^2 by a scaling factor 0.45 (Fang *et al.* 1996; Ji *et al.* 2016).

Data collection

Topographic and remote sensing data

The SRTM-DEM VERSION4 data were downloaded from the Shuttle Radar Topography Mission (SRTM) of the Consortium for Spatial Information website (CGIAR-CSI 2019). Data spatial resolution was 90 m, the projection method was Alberts, and the grid unit was resampled to 500 m. The 2018 land cover products (MCD12Q1, V055) and MODIS (Moderate-resolution Imaging Spectroradiometer) products were downloaded from the NASA Earth Observation System Data Service website (NASA 2019), and the land cover classification schema was that as defined by the IGBP (Table S2). The MODIS products used in this study are MOD09GA, MOD13Q1, MOD15A2, including Chinese image data from 2004 to 2018. Annual NDVI can be obtained by MRT (MODIS Reprojection Tools) splicing, conversion, projection, and other operations, and compounded according to the maximum value. After downloading directly on the Land Process Distributed Active Archive Centre of the US Geological Survey (LP DAAC), the MRT were used for processing, and the corresponding format conversion performed. Resampling with the nearest neighbour method was 1000x1000 m, the projection was converted to the Albers equal-area projection coordinate system, and the reference plane was Krasovsky 1940.

Meteorological data

The meteorological data from 2004 to 2018 for ~730 stations were downloaded from the China Meteorological Data Sharing Service System (CMDSS 2019). Data included daily values for precipitation, maximum and minimum temperature, and daily average temperature. Meteorological data were collated monthly to obtain average values for precipitation, total annual precipitation, monthly temperature, annual temperature and accumulated annual temperature above 0°C. All data were interpolated by ANUSPLIN (ver. 4.3, Centre for Research in Engineering Science, Australian National University, Canberra) (Hijmans *et al.* 2005; Zang 2014). ANUSPLIN was based on changes in geographic location and monthly average rainfall, which was a substitute for cloud cover which affects surface sunlight (McKenney *et al.* 2008).

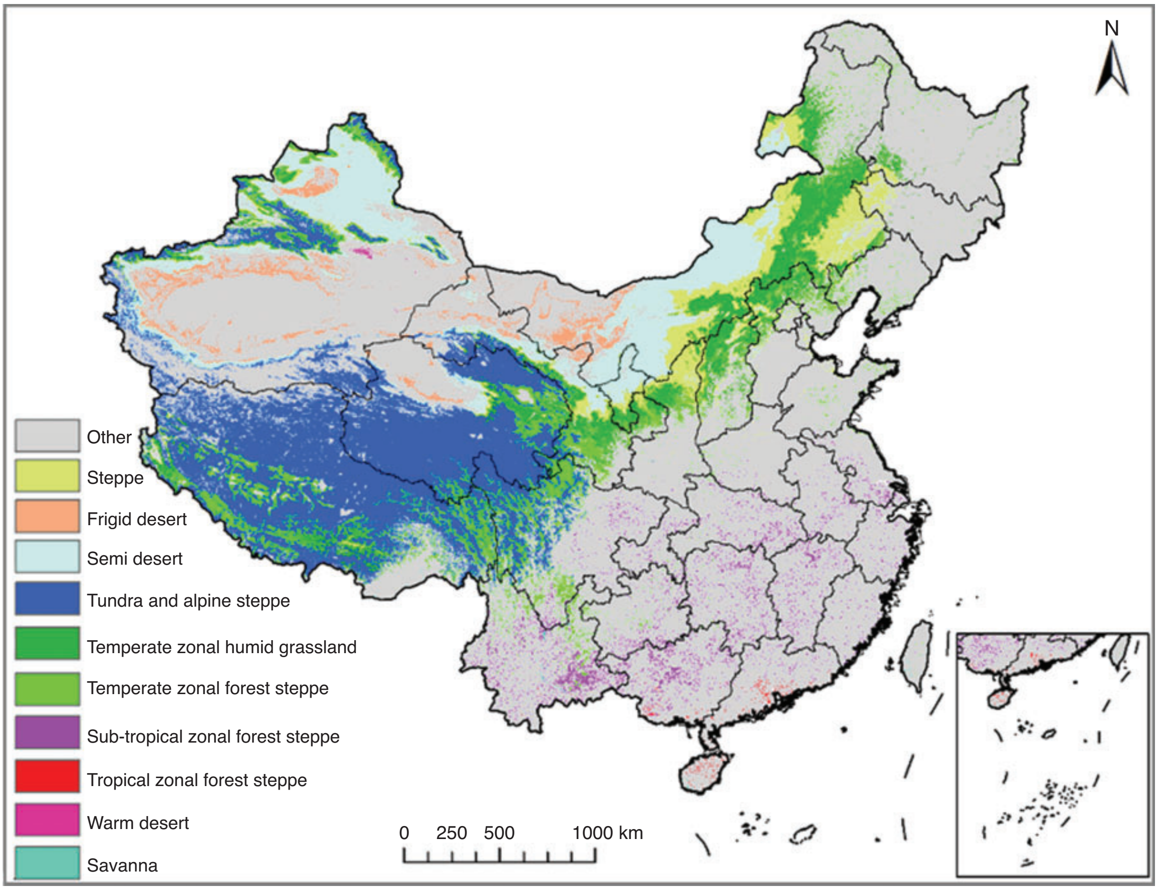

Fig. 2. The spatial distribution of grassland in China in 2018.

Research methods

Determination of grassland area

Based on the land use/land cover classification system proposed by IGBP, the global land was divided into 17 types including grassland (Table S2). The MODIS 2018 data (MCD12Q1 – see 'Topographic and remote sensing data') were used for classification processing. According to the MODIS IGBP land cover type merge plan (Table S3), we reclassified the IGBP data and superimposed the CSCS simulation results onto IGBP land cover type (Ren *et al.* 2008). The grassland super-class group database was assigned (Table S4) to obtain the 2018 grassland spatial distribution.

Determination of the optimal model

The Modified Classification Indices-based Models (MCIM). The construction of a new model used NDVI to modify the CIM, that was NPP = f(CIM × NDVI). The functional form refers to exponential, linear, linear binomial, logarithmic, and power models. Model construction and verification were all analysed and completed in STATA15 (STATA15 2017). Model construction was to randomly divide the NPP data of all measured samples into two parts, one (30%) of which was used for the construction of a new model, and the remainder (70%) used to validate the constructed model. We used 0.7 as the segmentation point of NDVI (Wang *et al.* 2019). When NDVI >0.7, vegetation coverage is high, it exhibits NDVI saturation (Duchemin *et al.* 2006; Gu *et al.* 2013).

Model comparison The NPP estimated values using Miami (Lieth 1972), Schuur (Schuur 2003), CIM (Lin *et al.* 2012, 2013*a*, 2013*b*), CASA (Hadian *et al.* 2019; Saki *et al.* 2019) and the new constructed models (mentioned above) were compared with NPP derived from measurements at 3360 sites in China, to evaluate the applicability and reliability of these NPP models.

Determination of the optimal model. The correlation coefficients R, R^2 and the root mean square error (RESE), and the ratio of the root mean square error to the measured average (RA) (Lin *et al.* 2012, 2013*b*), and the prediction efficiency E (Lin *et al.* 2013*a*) were all used to evaluate the simulation effect.

Determination of the spatial pattern of grassland NPP

Based on the 2018 grassland super-class group map and the optimal model, the spatial distribution pattern of NPP was to obtain through ArcGIS 10.5 software (ESRI Inc. 2017).

Results

Spatial distribution characteristics of grassland

In 2018, the total estimated area of grassland in China was 374.3 × 104 km^2. It is mainly distributed in north-western China (Fig. 2), accounting for ~90% of the total grassland area, the south-east accounts for the remainder. Tundra and alpine steppe occupy

Table 1. Statistics areas of among various super-class group in China in 2018

Super-class group	Area ($\times 10^4$ km^2)	The proportion of Chinese area (%)	The proportion of Chinese grassland area (%)
Tundra and alpine steppe	150.95	15.72	40.33
Frigid desert	15.97	1.66	4.27
Semi desert	63.89	6.66	17.07
Warm desert	0.19	0.02	0.05
Savanna	0.16	0.02	0.04
Steppe	38.25	3.98	10.22
Temperate humid grassland	50.85	5.29	13.59
Temperate forest steppe	42.93	4.47	11.47
Sub-tropical forest steppe	10.30	1.07	2.75
Tropical forest steppe	0.78	0.08	0.21

Table 2. Determination and verification of the Modified Classification Indices-based Models (MCIM)

Model name	Expression	R	R^2	RMSE	RA
Linear	$Y = \begin{cases} 0.843X + 70.291, NDVI < 0.7 \\ 0.408X + 222.96, NDVI \geq 0.7 \end{cases}$	0.5936	0.3523	122.93	0.5194
Linear binomial	$Y = \begin{cases} -0.002x^2 + 1.3608x + 46.785, NDVI < 0.7 \\ -0.0035x^2 + 2.0261x + 44.932, NDVI \geq 0.7 \end{cases}$	0.5912	0.3495	123.20	0.5205
Exponential	$Y = \begin{cases} 69.584 \times e^{0.0059X}, NDVI < 0.7 \\ 197.69 \times e^{0.0015X}, NDVI \geq 0.7 \end{cases}$	0.5769	0.3328	124.76	0.5271
Logarithm	$Y = \begin{cases} 70.639 \times \ln X - 151.78, NDVI < 0.7 \\ 92.781 \times \ln X - 185.24, NDVI \geq 0.7 \end{cases}$	0.5913	0.3497	123.18	0.5204
Power	$Y = \begin{cases} 12.554 \times X^{0.5308}, NDVI < 0.7 \\ 44.421 \times X^{0.3396}, NDVI \geq 0.7 \end{cases}$	0.5968	0.3562	122.56	0.5178
Log power	$\ln Y = \begin{cases} 2.533 \times \ln X^{0.4391}, NDVI < 0.7 \\ 3.2056 \times \ln X^{0.3314}, NDVI \geq 0.7 \end{cases}$	0.5965	0.3559	122.59	0.5179

the largest area (Table 1), accounting for 40.3% of the total area, mainly distributed in the Qinghai-Tibet Plateau, Qinghai Province, and Xinjiang Uygur Autonomous Region (Fig. 2); followed by semi desert distributed in northern China, including Inner Mongolia, Xinjiang and elsewhere (Fig. 2). The total area of steppe and temperate humid grassland was projected to be 89.1 $\times$ 104 km^2, accounting for 23.8% of the total grassland area, with nearly half distributed on the Inner Mongolian Plateau. Warm desert and Savanna recorded the smallest proportions (Table 1). Savanna and warm desert were projected to cover $<$0.35 $\times$ 104 km^2. Savanna was projected to be located in southern China, particularly in Hainan Province, and warm desert projected to be located in the Tarim Basin in Xinjiang Uygur Autonomous Region and the Qaidam Basin in Qinghai Province (Fig. 2).

Determination of the optimal model

The optimal MCIM. The power function model was the optimal selection for the MCIM, constructed using 30% of the measured data, with 70% of the data used for validation. For R^2, NPP power $>$ NPP Log power $>$ NPPLinear $>$ NPPlogarithm $>$ NPPLinear binomial $>$ NPPexponential; for RA, NPP power $<$ NPP Log power $<$ NPP Linear $<$ NPP logarithm $<$ NPP Linear binomial $<$ NPP exponential. It was determined that the power function model had the best simulation effect (Table 2).

Model comparison and validation

The optimal MCIM was the optimal model, which greatly improved the simulation accuracy of NPP compared with other models (Table 3). For R^2, NCASA $>$ NOptimal MCIM $>$ NCIM $>$ NSchuur $>$ NMiami; for RMSE (Fig. 3), NMiami $>$ NCIM $>$ NSchuur $>$ NCASA $>$ NOptimal MCIM; for E, NOptimal MCIM $>$ NCASA $>$ NCIM $>$ N Schuur $>$ NMiami. The optimal MCIM model had the highest prediction efficiency, which was closest to the measured value of NPP, and the Miami simulation effect had the lowest (Fig. 3; Table 3).

Spatial distribution pattern of grassland NPP

The grassland NPP was projected to increase from north-west China to the south-east, corresponding with changes in precipitation and temperature. The total NPP (TNPP) of grassland provided was 388.04 $\times$ 10^{12} g C/year in 2018 (Fig. 4).

Table 3. Comparison between NPP models

NPP model	R	R^2	RMSE	E
CASA	0.62	0.39	126.01	0.23
CIM	0.44	0.19	145.64	0.18
Schuur	0.43	0.18	145.57	0.10
MIAMI	0.39	0.15	148.71	0.09
Optimal MCIM	0.60	0.36	122.56	0.32

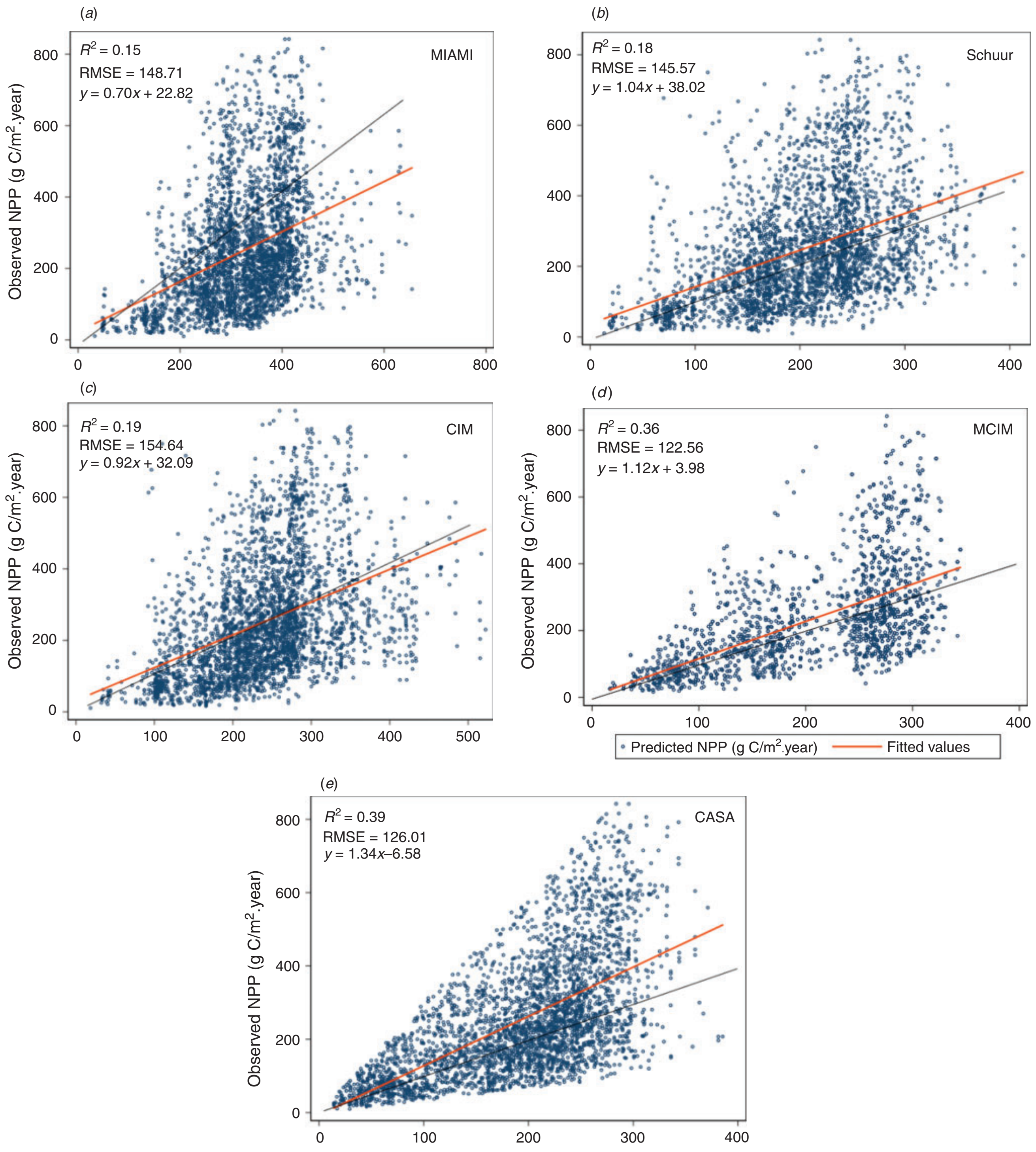

Fig. 3. Comparison the NPP estimates of Miami, Schuur, CIM, Optimal MCIM and CASA models. The red line represents the fitted linear regression line. The black line is a 1:1 scale line.

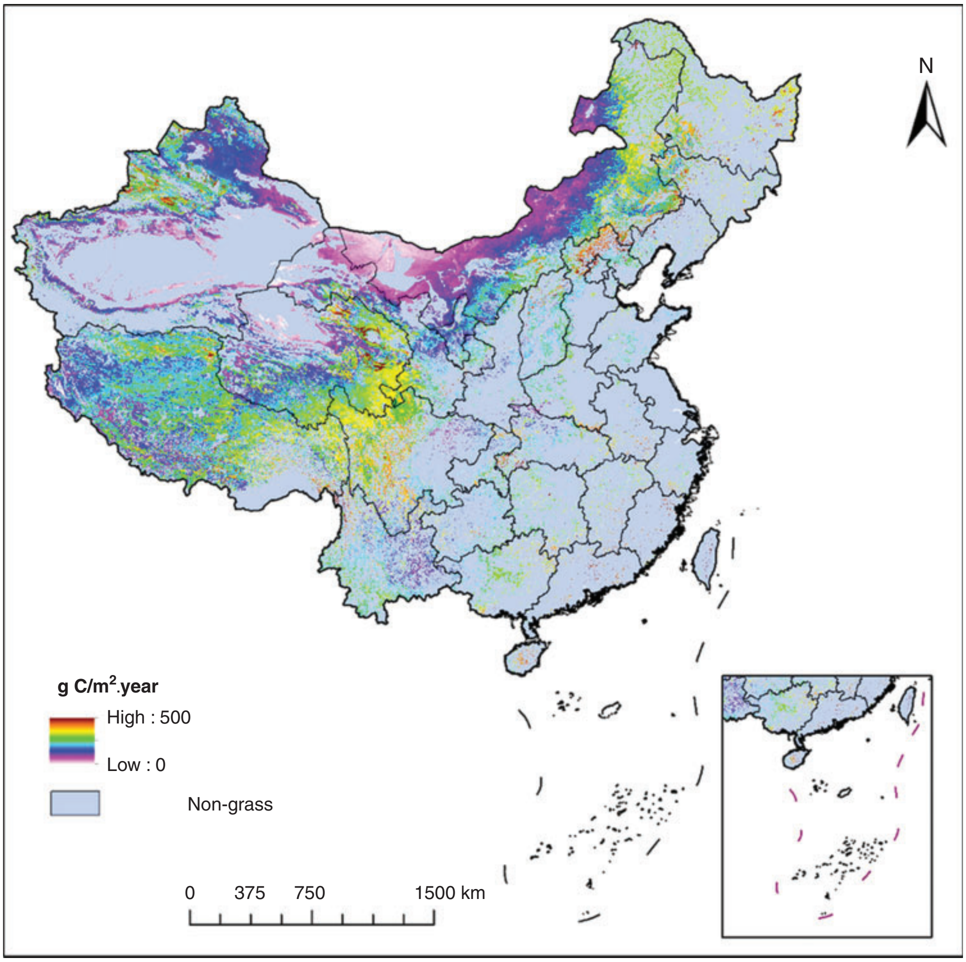

Fig. 4. Spatial distributions of grassland NPP in China in 2018.

Table 4. Statistics NPP among various super-class group in China in 2018

Super-Class group	Minimum NPP (g C/m^2.year)	Maximum NPP (g C/m^2.year)	Mean NPP (g C/m^2.year)	Total NPP ($\times 10^{12}$ g C/year)
Tundra and alpine steppe	0.00	414.07	136.30	153.49
Frigid desert	0.06	253.15	56.78	5.46
Semi desert	0.00	415.67	97.71	50.12
Warm desert	0.01	121.60	17.32	0.012
Savanna	20.16	425.78	325.57	0.18
Steppe	2.10	421.47	165.00	37.97
Temperate humid grassland	0.00	415.17	194.24	59.00
Temperate forest steppe	0.00	463.03	231.67	61.84
Sub-tropical forest steppe	0.00	477.74	367.16	19.07
Tropical forest steppe	0.00	476.76	400.25	0.90

Comparison the NPP maps in Fig. 4 with data in Table 4 shows that the highest TNPP values of grassland super-class groups were projected to be in the tundra and alpine steppe (153.5×10^{12} g C), followed by temperate forest steppe (61.8×10^{12} g C), and temperate humid grassland (59.0×10^{12} g C), respectively. Although tundra and alpine steppe has lower NPP values than temperate humid grassland on a unit-area basis, the TNPP for tundra and alpine steppe was projected to be more than twice that of temperate humid grassland, because tundra and alpine steppe was projected to cover a greater area (Table 1). Warm desert and savanna were projected to have the lowest TNPP, and semi-desert and frigid desert to have moderate TNPP values (Table 4).

Discussion

The combination of IGBP and CSCS has obvious advantages in calculating the grassland area

The combination of IGBP and CSCS for calculating the grassland area was accurate and had a solid foundation. The IGBP and the International Human Dimensions Program on Global Environmental Change (IHDP) jointly proposed the Land Use and Land Cover Change Research Program, the LUCC, which defined land cover as 'the natural state of Earth's land surface, which was the natural result of natural processes and human activities' (Turner *et al.* 1995; Friedl *et al.* 2002). The CSCS can also be used to determine the grassland area, and has been widely used since it was proposed. Xiu *et al.* (2014) used the land cover classification data (MCD12Q1) combined with the CSCS method and estimated a minimum potential Chinese grassland area of 0.0137 km^2. The grassland area calculated in this study was less than the above result, because IGBP and CSCS calculated the actual grassland area in China. Based on China's land cover data, Fang *et al.* (2018) used the relationship between precipitation and NDVI to obtain an average total grassland area of 293.05×104 km^2 between 1982 and 2011. This result was less than that obtained in this study, because their result was an averaged value over 30 years, and where NDVI < 0.1, they regarded the area as desert. When NDVI < 0.1, the land included desert and desert steppe (Zhang *et al.* 2009). However, Fang's method was too mechanical to judge directly using NDVI and classify the desert steppe as desert, so the result was less than calculated in this study. The combination of grassland type and land use type was more accurate for the actual situation of desert grassland usage.

The combination of CSCS and IGBP-LUCC provided the operational feasibility for exploring the spatial and temporal distribution pattern of grassland types. Determining the area of grassland not only achieves area attributes, but also type attributes, which enriches the diversity of calculation. Using a combination of IGBP and CSCS, this study calculated the grassland area in China and the 10 grassland super-class groups, achieved the calculation of the spatial distribution of grassland.

The optimal MCIM realises the accurate calculation of grassland NPP

The optimal MCIM was superior to both the Miami and Schuur, and lower than the CASA. The implementation of the CASA model requires multiple conversions, which invariably increases the error and reduces the simulation accuracy. The optimal MCIM has a simple structure, is technically easier to implement, and its required indicators are easily obtained, so that it is easier to handle and can accomplish NPP estimation on a large regional scale. The TNPP of 4.9 Pg C/year in China was calculated using the NDVI dataset and modified CASA (Zhang *et al.* 2016). The TNPP calculated in this study was less than the above results, because these results considered the impact of precipitation on the distribution of grassland NPP, and added numerous parameters. In this study, according to the optimal MCIM calculation, the TNPP in 2018 was less than the highest value of the previous study, the TNPP in the grassland was less than that in the potential grassland area, and the number of model conversions was lower, improving the accuracy. The optimal MCIM model was not only applicable to the conditions of developing countries, but also laid the foundation for accurately calculating the NPP of each grassland super-class group.

A new strategy for grassland classification management

Grazing intensity can change the surface landscape and affect regional productivity (Köchy *et al.* 2008). The rational arrangement of the ecological and production functions (available aboveground biomass) provided by grasslands can be evaluated based on indicators such as the theoretical carrying capacity on different grassland super-class groups. The theoretical carrying capacity refers to the number of livestock that can be grazed per unit area of grassland under moderate grazing. It is one of the main indicators of grassland productivity. It can be evaluated according to the growth of forage (including forage quality and yield), which depends on the primary productivity of the grassland. We used the theoretical carrying capacity formula (Fang *et al.* 1996; Su *et al.* 2013; Table S1). Variables such as grassland utilisation rate of different types of forages (Chen 2001) and daily feed per unit of livestock (Chen 2001), for example, can be used to calculate the livestock carrying capacity per unit area of grassland in China in 2018 (Table 5). The sustainable development of grassland resources requires a rational arrangement of grassland ecological and productive functions (Fig. 5). A large area in northern China, especially Inner Mongolia, has a low number of animals per unit area. This area should focus on its ecological services, and protect the ecology through measures such as grazing prohibition. The theoretical animal carrying capacity in south-east Qinghai and north-west Sichuan is relatively high, and can be used as a production function service area for grazing. The Qinghai-Tibet Plateau is a key area for ecological functions, and strict grazing bans should be implemented to protect the ecology. The north-east area has a high carrying capacity per unit area, and can be used as a production function service, and the north-east area had high vegetation coverage and rich vegetation types for livestock to forage (Fig. 5).

To balance grassland productive and ecological function, it is necessary to determine which function is more suitable for each grassland super-class group. Statistics on grassland productivity of various grassland super-class groups (Table 5) indicated that the total belowground biomass of TNPP was 333.1×10^{12} g C, and available aboveground biomass was 33.3×10^{12} g C, and the total theoretical carrying capacity was 10062.7×104 sheep units including five super-class groups with more than 10 million sheep units. This suggests that the tundra and alpine steppe, semi desert, steppe, temperate humid grassland, and temperate forest steppe were the main types of available grassland.

With respect to available biomass productive efficiency, efficiency of grassland such as steppe, temperate humid grassland, and temperate forest steppe was high. The belowground biomass of tundra and alpine steppe was up to 134.1×10^{12} g C, and the production efficiency of available biomass per unit area 7.4%. The belowground biomass of herbage accounted for more than 80% of the total biomass. However, the aboveground biomass can be used by livestock for a short time with low efficiency, which reflected that the major function of tundra and

Table 5. Statistics on grassland productivity among various grassland super-class groups in 2018

Super-Class group	Belowground biomass ($\times 10^{12}$ g C)	Available aboveground biomass ($\times 10^{12}$ g C)	Production efficiency of available biomass (%)	Theoretic carrying capacity ($\times 10^4$ sheep unit)
Tundra and alpine steppe	134.09	11.09	7.35	3725.51
Frigid desert	4.79	0.40	2.50	122.88
Semi desert	43.82	5.24	8.20	1085.38
Warm desert	0.002	0.009	4.74	0.33
Savanna	0.15	0.018	11.25	6.15
Steppe	31.64	3.57	9.33	1102.18
Temperate humid grassland	49.26	5.49	10.80	1699.38
Temperate forest steppe	53.01	5.39	12.56	1660.34
Subtropical forest steppe	15.64	1.96	19.03	630.50
Tropical forest steppe	0.74	0.095	12.18	30.08
Total	333.142	33.262	100	10062.73

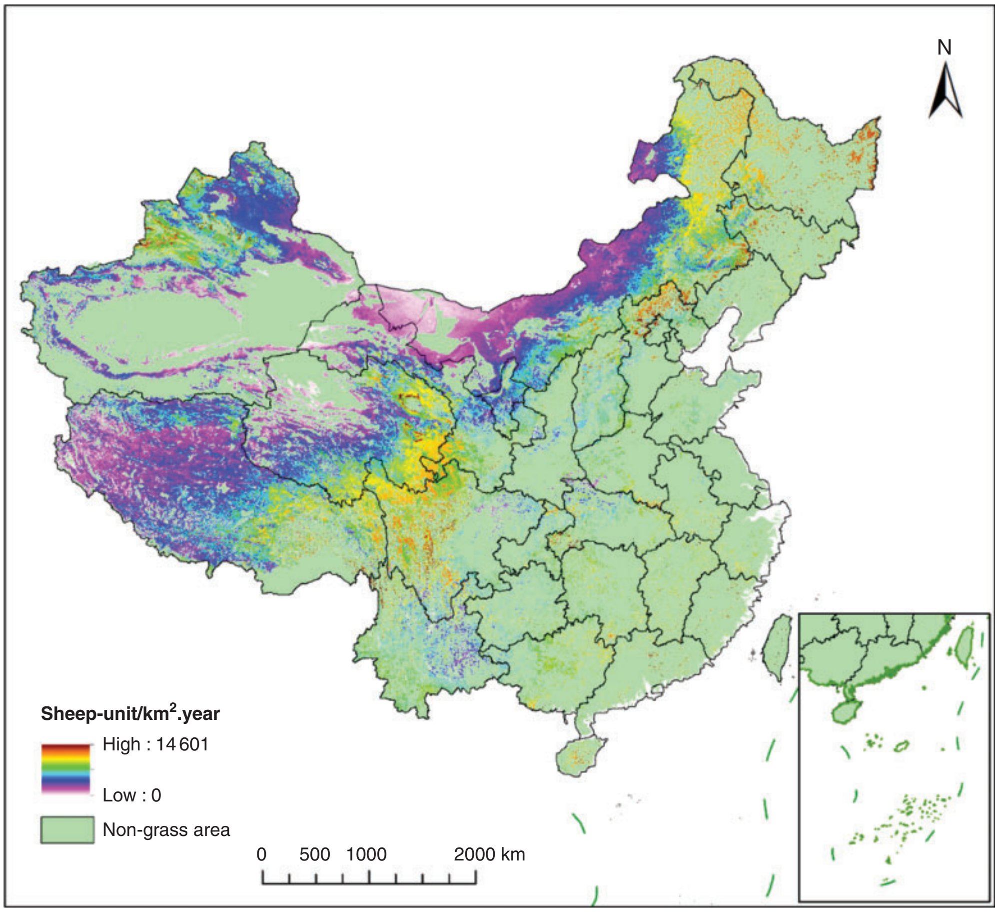

Fig. 5. Theoretic carrying capacity in China in 2018.

alpine steppe was ecological rather than productive (Table 5). The belowground biomass of the steppe was 31.6×10^{12} g C, the available aboveground biomass 3.6×10^{12} g C, and the production efficiency 9.3%. This implies that productive and ecological functions are equally important for steppe. Meanwhile, the temperate humid grassland, temperate forest steppe, and subtropical forest steppe had higher available aboveground biomass, and consequently their productive functions were more prominent.

Conclusions

This study explains the actual spatial distribution of grassland through the combination of IGBP and CSCS. The total area of grassland was $\sim 374.3 \times 104$ km^2 in China in 2018, which was mainly distributed in north-western China. The optimal MCIM had the highest prediction efficiency, and the overall accuracy was higher than the standard classical model (Miami, Schuur, CIM, and CASA models). It accomplished the accurate calculation of grassland NPP in China. Based on the optimal model as the algorithm basis, the total NPP was 388.04×10^{12} g C/year in the study area in 2018. The results have provided a basis for the rational arrangement of grassland ecological and productive functions, and have been significant in developing a new strategy of grassland classification management in China.

Conflicts of interest

Huilong Lin is a Guest Associate Editor of the *Rangeland Journal* but was blinded from the peer-review process for this paper. The authors declare no other conflicts of interest.

Acknowledgements

This work was supported by the National Natural Science Foundation of China (31772666), the National Key Research and Development Plan (2016YFC0501906), the Fundamental Research Funds for the Central University (lzujbky-2020-kb29), and the Key Consulting Project of the Chinese Academy of Engineering (2020-XZ-29).

References

CGIAR-CSI (2019). SRTM 90m Digital Elevation Database ver. 4.1. Available at: http://srtm.csi.cgiar.org/SELECTION/inputCoord.asp (accessed 25 June 2019).

Chen, B. M. (2001). 'China's Comprehensive Agricultural Resources Production Capacity and Population Carrying Capacity.' (China Meteorological Press: Beijing.) [in Chinese]

CMDSS (2019). China Meteorological Data Sharing Service System. The meteorological data. Available at: http://data.cma.cn/data/online/t/1 (accessed 25 June 2019).

de Beurs, K. M., and Henebry, G. M. (2005). Land surface phenology and temperature variation in the international geosphere-biosphere program high-latitude transects. *Global Change Biology* **11**, 779–790. doi:10.1111/j.1365-2486.2005.00949.x

Duchemin, B., Hadria, R., Erraki, S., Boulet, G., Mawasongrande, P., Chehbouni, A., Escadafal, R., Ezzahar, J., Hoedjes, J. C. B., Kharrou, M. H., Khabba, S., Mougenot, B., Olioso, A., Rodriguez, J. C., and Simonneaux, V. (2006). Monitoring wheat phenology and irrigation in Central Morocco: On the use of relationships between evapotranspiration, crops coefficients, leaf area index and remotely-sensed vegetation indices. *Agricultural Water Management* **79**, 1–27. doi:10.1016/j.agwat.2005.02.013

ESRI Inc. (2017). ArcGIS10.5. Available at: https://www.esri.com/en-us/home

Fang, J. Y., Liu, G. H., and Xu, S. L. (1996). Biomass and net production of forest vegetation in China. *Acta Ecologica Sinica* **16**, 497–508 [in Chinese].

Fang, J. Y., Geng, X. Q., Zhao, X., Shen, H. H., and Hu, H. F. (2018). How many areas of grasslands were there in China? *Chinese Science Bulletin* **63**(17), 1731–1739. doi:10.1360/N972018-00032 [in Chinese]

Feng, Q. S., Liang, T. G., Huang, X. D., Lin, H. L., Xie, H. J., and Ren, J. (2013). Characteristics of global potential natural vegetation distribution from 1911 to 2000 based on comprehensive sequential classification system approach. *Grassland Science* **59**, 87–99. doi:10.1111/grs.12016

Friedl, M. A., Gopal, S., Muchoney, D., and Strahler, A. H. (2002). Global land cover mapping from MODIS: algorithm design and preliminary results. *In*: 'IEEE International Geoscience and Remote Sensing Symposium'. (IEEE.) doi:10.1109/IGARSS.2000.861618

Gu, Y. X., Wylie, B. K., Howard, D. M., Phuyal, K. P., and Ji, L. (2013). NDVI saturation adjustment: A new approach for improving cropland performance estimates in the Greater Platte River Basin, USA. *Ecological Indicators* **30**, 1–6. doi:10.1016/j.ecolind.2013.01.041

Hadian, F., Jafari, R., Bashari, H., Tartesh, M., and Clarke, K. D. (2019). Estimation of spatial and temporal changes in net primary production based on Carnegie Ames Stanford Approach (CASA) model in semi-arid rangelands of Semirom County, Iran. *Journal of Arid Land* **11**, 477–494. doi:10.1007/s40333-019-0060-3

Han, Z., Song, W., Deng, X. Z., and Xu, X. L. (2018). Grassland ecosystem responses to climate change and human activities within the Three-River Headwaters region of China. *Scientific Reports* **8**, 9079–9092. doi:10.1038/s41598-018-27150-5

Hijmans, R. J., Cameron, S. E., Parra, J. L., Jones, P. G., and Jarvwas, A. (2005). Very high resolution interpolated climate surfaces for global land areas. *International Journal of Climatology* **25**, 1965–1978. doi:10.1002/joc.1276

Hou, X. Y. (2001). China Vegetation Atlas (11 million) published in April 2001. *Acta Phytoecologica Sinica* (03), 343 [in Chinese].

Jay, S., Potter, C., Crabtree, R., Genovese, V., Weiss, D. J., and Kraft, M. (2016). Evaluation of modeled net primary production using MODIS and Landsat satellite data fusion. *Carbon Balance and Management* **11**, 8–21. doi:10.1186/s13021-016-0049-6

Ji, W. J., Li, S., Chen, S. C., Shi, Z., Vwascarra Rossel, R. A., and Mouazen, A. M. (2016). Prediction of soil attributes using the Chinese soil spectral library and standardized spectra recorded at field conditions. *Soil & Tillage Research* **155**, 492–500. doi:10.1016/j.still.2015.06.004

Köchy, M., Mathaj, M., Jeltsch, F., and Malkinson, D. (2008). Resilience of stocking capacity to changing climate in arid to Mediterranean landscapes. *Regional Environmental Change* **8**, 73–87. doi:10.1007/s10113-008-0048-6

Li, K. R., Wang, S. Q., and Cao, M. K. (2004). Vegetation and soil carbon storage in China. *Science in China. Series D, Earth Sciences* **47**, 49–57. doi:10.1360/02yd0029 [in Chinese]

Liang, T. G., Feng, Q. S., Cao, J., Xie, H., Lin, H. L., Zhao, J., and Ren, J. Z. (2012*a*). Changes in global potential vegetation distributions from 1911 to 2000 as simulated by the Comprehensive Sequential Classification System approach. *Chinese Science Bulletin* **57**, 1298–1310. doi:10.1007/s11434-011-4870-8

Liang, T. G., Feng, Q. S., Yu, H., Huang, X. D., Lin, H. L., Sha, Z. A., and Ren, J. Z. (2012*b*). Dynamics of natural vegetation on the Tibetan Plateau from past to future using a comprehensive and sequential classification system and remote sensing data. *Grassland Science* **58**, 208–220. doi:10.1111/grs.12000

Lieth, H. (1972). Modelling the primary productivity of the world. *Natural Resources* **8**, 5–10.

Lin, H. L., Zhao, J., Liang, T. G., Bogaert, J., and Li, Z. Q. (2012). A Classification indices-based model for net primary productivity (NPP) and potential productivity of vegetation in China. *International Journal of Biomathematics* **5**, 1260009. doi:10.1142/S1793524512600091

Lin, H. L., Wang, X. L., Zhan, Y. J., Liang, T. G., Feng, Q. S., and Ren, J. Z. (2013*a*). Spatiotemporal dynamics on the distribution, extent and NPP of potential grassland in response to climate changes in China. *The Rangeland Journal* **35**, 409–425. doi:10.1071/RJ12024

Lin, H. L., Feng, Q. S., Liang, T. G., and Ren, J. Z. (2013*b*). Modelling global-scale potential grassland changes in spatio-temporal patterns to global climate change. *International Journal of Sustainable Development and World Ecology* **20**, 83–96. doi:10.1080/13504509.2012.749815

Liu, Y. Y., Wang, Q., Zhang, Z. Y., Tong, L. J., Wang, Z. Q., and Li, J. L. (2019). Grassland dynamics in responses to climate variation and human activities in China from 2000 to 2013. *The Science of the Total Environment* **690**, 27–39. doi:10.1016/j.scitotenv.2019.06.503

Long, S. P., Garcia Moya, E., Imbamba, S. K., Kamnalrut, A., Piedade, M. T. F., Scurlock, J. M. O., Shen, Y. K., and Hall, D. O. (1989). Primary productivity of natural grass ecosystems of the tropics: a reappraisal. *Plant and Soil* **115**, 155–166. doi:10.1007/BF02202584

Ma, A., He, N., Yu, G., Wen, D., and Peng, S. (2016). Carbon storage in Chinese grassland ecosystems: Influence of different integrative methods. *Scientific Reports* **6**, 21378. doi:10.1038/srep21378

Matsushita, B., Xu, M., Chen, J., Kameyama, S., and Tamura, M. (2004). Estimation of regional net primary productivity (NPP) using a process-based ecosystem model: How important was the accuracy of climate data? *Ecological Modelling* **178**, 371–388. doi:10.1016/j.ecolmodel.2004.03.012

McKenney, D. W., Pelland, S., Poissant, Y., Morris, R., Hutchinson, M., Papadopol, P., Lawrence, K., and Campbell, K. (2008). Spatial insolation models for photovoltaic energy in Canada. *Solar Energy* **82**, 1049–1061. doi:10.1016/j.solener.2008.04.008

Monteith, J. K. (1972). Solar radiation and productivity in tropical ecosystems. *Journal of Applied Ecology* **9**, 747–766. doi:10.2307/2401901

National Aeronautics and Space Administration (NASA) (2019). The MODIS Land Products [WWW Document]. National Aeronaut. Sp. Adm. L. Process. Distribution Act. Arch. Center Land Processes Distributed Active Archive Center (LP DAAC). Available at: https://lpdaac.usgs.gov/product_search/?keyword=Land+Cover&view=list&sort=title (accessed 25 June 2019).

Ni, J. (2002). Carbon storage in grasslands of China. *Journal of Arid Environments* **50**, 205–218. doi:10.1006/jare.2001.0902

Piao, S. L., Fang, J. Y., He, J. S., and Xiao, Y. (2004). Spatial distribution of grassland biomass in China. *Acta Phytoecologica Sinica* **28**, 491–498 [in Chinese].

Ren, J. Z., Hu, Z. Z., Zhao, J., Zhang, D. G., Hou, F. J., Lin, H. L., and Mu, X. D. (2008). A grassland classification system and its application in China. *The Rangeland Journal* **30**, 199–209. doi:10.1071/RJ08002

Rosswall, T. (1992). The international geosphere-biosphere programme: a study of global change (IGBP). *Environmental Geology and Water Sciences* **20**, 77–78. doi:10.1007/BF01737873

Saki, M., Soltani, S., Esfahani, M. T., and Jafari, R. (2019). Evaluating the variability of ANPP in central Iranian arid and semi-arid rangelands using CASA model and its relationship with climatic factors. *Geosciences Journal* **23**(3), 531–545. doi:10.1007/s12303-018-0040-1

Schuur, E. A. G. (2003). Productivity and global climate revisited: the sensitivity of tropical forest growth to precipitation. *Ecology* **84**, 1165–1170. doi:10.1890/0012-9658(2003)084[1165:PAGCRT]2.0.CO;2

Shen, H. H., Zhu, Y. K., Zhao, X., Geng, X. Q., Gao, S. Q., and Fang, J. Y. (2016). Analysis on the present situation of grassland resources in China. *Chinese Science Bulletin* **61**, 139–154 [in Chinese].

STATA15 (2017). STATA Crop. Available at: https://www.stata.com/.

Su, R. N., Zu, J. X., Jin, H., Chao, L. M. Q. Q. G., Wang, Z. J., Cha, M. H., Na, Y., and Li, J. Q. (2013). Changes in grassland productivity and livestock carrying capacity in Inner Mongolia. *Ecology & Environment* **26**, 605–612 [in Chinese].

Sun, S. Z. (1981). Introduction to vegetation map of the People's Republic of China (1:4000000). *Acta Phytoecologia Et Geobotaniga Ginica* **5**, 79 [in Chinese].

Tripathi, P., Patel, N. R., and Kushwaha, S. P. S. (2018). Estimating net primary productivity in tropical forest plantations in India using satellite-driven ecosystem model. *Geocarto International* **33**, 988–999. doi:10.1080/10106049.2017.1323963

Turner, B. L., Skole, D. L., Sanderson, S., Fischer, G., Fresco, L., and Leemans, R. (1995). Land-use and land-cover change. Science / research plan. *Global Change Report* **43**, 669–679.

Wake, B. (2014). Looking forward. *Nature Climate Change* **4**, 856–857. doi:10.1038/nclimate2395

Wang, S. Y., Liu, J. Y., Zhang, Z. X., Zhou, Q. B., and Zhao, X. L. (2001). Analysis of the characteristics of land use in China. *Acta Geographica Sinica* **56**, 631–639 [in Chinese].

Wang, C., Lin, H. L., and Zhao, Y. T. (2019). A modification of CIM for prediction of net primary productivity of the Three-River Headwaters, China. *Rangeland Ecology and Management* **72**, 327–335. doi:10.1016/j.rama.2018.11.003

Xiao, X. Y., Li, X. B., Jiang, T., Tan, M. H., Hu, M. Y., Liu, Y. Q., and Zeng, W. (2019). Response of net primary production to land use and climate changes in the middle reaches of the Heihe River Basin. *Ecology and Evolution* **9**, 4651–4666. doi:10.1002/ece3.5068

Xiu, L. N., Feng, Q. S., Liang, T. G., and Ren, J. Z. (2014). Spatial and temporal distribution of grassland and human occupancy condition in China from 2001 to 2009. *Pratacultural Science* **31**, 66–74 [in Chinese].

Zang, C. L. (2014). Research temperature and precipitation interpolation methods of China. Shandong Agricultural University, DC. [in Chinese]

Zhang, M. L., Jiang, W. L., Cheng, Q. Q., Zhao, Y. Y., and Liu, X. N. (2011). Research progress in the estimation models of grassland net primary productivity. *Acta Agrestia Sinica* **19**, 356–366 [in Chinese].

Zhang, H. B., Yang, G. X., Wu, W. B., Li, G., Chen, B. R., and Xin, X. P. (2009). Spatiotemporal characteristics of modis ndvi in hulunber grassland. *The Journal of Applied Ecology* **20**, 2743–2749.

Zhang, M. L., Lal, R., Zhao, Y. Y., Jiang, W. L., and Chen, Q. G. (2016). Estimating net primary production of natural grassland and its spatio-temporal distribution in China. *The Science of the Total Environment* **553**, 184–195. doi:10.1016/j.scitotenv.2016.02.106

Zhu, W. Q., Cheng, Y. H., Xu, D., and Li, J. (2005). Advances in terrestrial net primary productivity (NPP) estimation models. *Chinese Journal of Ecology* **24**, 296–300 [in Chinese].